Modified Surface Nanoscale Explosion: Effects of Initial Condition and Charge Flow

Magnus Hedström and Hai-Ping Cheng*

Department of Physics and Quantum Theory Project, University of Florida, Gainesville, Florida 32611

Received: June 15, 1999; In Final Form: March 1, 2000

Molecular dynamics (MD) simulations have been performed to study surface nanoscale explosion due to *slow* highly charged ion (HCI)−surface interactions. In order to understand the interplay between the mechanisms for surface modification and the dynamical consequences of the explosion, a new simulation model is formulated to include the electronic degrees of freedom in an empirical manner. In this model, surface ionization occurs at a finite rate and surface charges are allowed to flow into the substrate at various rates simultaneously. In one of the simulations based on the simultaneous ionization and charge migration (SICM) model, 100 excitations (positively charged surface ions) occur during the first 24 fs, which is longer than the in-the-substrate neutralization time of the HCI (approximately 10 fs) deduced from experimental measurements. At the same time, positively charged surface ions are allowed to migrate away from the center region at an average speed of approximately 40 Å per picosecond. Compared to the results from pure Coulomb explosion in which charge exchange between surface atoms and surface ion is not allowed, the strength of the nano-explosion is not weakened but somewhat enhanced. When the time interval for ionization is reduced to instant charging but with other conditions unchanged, little influence on the formation of a crater was found between the two cases. The finite time interval for building up the charged region only postponed the formation of the repulsive center by approximately 25 fs and slightly lowered the peak value of the Coulomb repulsion. The explosion strength starts to decrease, however, as the speed of the charge flow in the substrate increases. In a test simulation, an estimation of a lower bound of surface damage as a function of surface energy deposition is provided by monitoring the dynamics according to the energetics of the systems. Dynamical consequences of these surface processes are studied by a comprehensive analysis of energetics, temperature, pressure, and structural information. We also discuss the relevance of the current model to HCI−surface experiments as well as to future modeling and simulations.

I. Introduction

Highly charged ion (HCI)−surface interactions have become a subject of interest in recent years, because of advances in the electron beam ion trap (EBIT) technology.[1−14] During the ion−surface impact, a large amount of energy that is initially stored in the form of electrostatic potential energy (as opposed to conventional swift ions that have high kinetic energy) is redistributed through various complex channels. Many physical phenomena, including formation of hollow atoms in which electrons occupy highly excited states, Auger cascades, and emission of secondary particles (electrons, ions, atoms, clusters, and X-rays), are observed when a *slow* ($v \sim 10^4-10^6$ m/s) HCI (with charge state $q = +44$ to $+92$) approaches the surface. In particular, a large number of electrons (more than $4q$), are emitted from the surfaces. The patterns of secondary ion emission spectrometry (SIMS) are found to be highly sensitive to the charge states of the projectile ion. The sputtering process caused by HCI surface interaction is now known as potential energy sputtering or sometime electronic sputtering. The dynamical response in the lattice to the incident ions varies according to the material characteristics of the target substrate. The HCI−surface interactions are known to cause permanent damage to insulators such as SiO_2,[2,4−6,10,15] to metal oxides,[2,4,16] and to ionic crystals (LiF),[17,18] while no visible lattice defects have been observed in metallic substrates.[4,19] In order to explain the formation of nanosize craters on the surface, a Coulomb explosion model[2,20,21] as well as a defect-mediated model[15,16,22] have been presented as possible mechanisms for a surface explosion that causes the formation of surface nanostructures during the HCI bombardment.

Semiconductor surfaces have raised some controversial issues over the last 10 years, thus attracting most of the current interest in HCI−surface experimental studies.[23−26] Early measurements were mostly performed using ions of relatively low charge ($q < +10$). An experimental group in Japan[27,28] reported evidence of charge dependency of secondary ion emission during ion−GaAs surface interactions, while other experiments[29] have shown that under the low charge state condition, neither surface damage nor charge state dependency was observed in ion−silicon surface interactions. Recently, two EBIT groups, at the National Institute of Standards and Technology (NIST) and at the Lawrence Livermore National Laboratory (LLNL), have developed techniques for studying HCI−Si surface bombardment using ions with ultrahigh charge states ($q = +44$, $+76$, etc.). A similar device has also been employed at LLNL for GaAs surface studies. These experiments indicate strong dependence of the final surface morphology on the charge state of the projectile ions. The Si surface shows clearly roughness after bombardment with Xe^{44+},[25] although the formation mechanisms remain to be discovered. For GaAs, 1400 GaAs atoms/per HCI are emitted

* Corresponding author.

10.1021/jp993283u CCC: $19.00
Published on Web 04/19/2000

from the substrate during the potential energy (or electronic) sputtering processes,[23] which leads to the suggestion of a bond-breaking mechanism[30−32] which also results surface damage.

These results have revealed the complexity of the potential energy sputtering mechanisms that lead to highly nontrivial outcomes. For example, the ratio of the number of emitted ions to the neutral species does not always increase as q increases.[23] A major question has also arisen from the experiments regarding the energy redistribution during the ion−surface interaction. After adding up all the energies that cause electron emission, X-ray and atom/ion emission, electron−hole pair in the substrate, a large amount of energy remains missing from the estimation and needs to be identified.[25] These questions and puzzles are partially due to the lack of information on the surface structural modification.

To understand the dynamics of surface particles (atoms and ions) and surface modification processes, we formulated theoretical models for molecular dynamics (MD) simulations to study the above-mentioned surface processes. Our first molecular dynamics simulations[33,34] were based on instantaneous charging and frozen state (ICFS) model that assumes instant surface ionization and does not allow a surface ion or atom to change its charge states. Up to date, most theoretical studies that have provided important physical insights focused on the electronic state of the projectile ions, or the emission rates of electrons, X-rays, etc. The dynamics of the surface atoms that is directly related to the formation of surface structures had been described only in a qualitative, phenomenological, manner. In the analyses of secondary particle (atoms and ions) emission, the low ion-to-neutral ratio was used as evidence against the Coulomb explosion model.[22] Nevertheless, the simulations show that ion-to-neutral ratio is low even when Coulomb explosion is the dominant mechanism.[33,34]

Even though the MD method has been used extensively in the studies of a wide range of physical phenomena, its application in the area of HCI−surface interaction is far underrepresented. The difficulties to properly applying MD to these types of phenomena come from the fact that the electronic excitation and the nuclear motion are entangled during the sputtering processes. In ion−surface interaction, we have a highly nonequilibrium situation, and a multitude of excitation and relaxation processes are possible. Practical simulation models that can properly separate and recombine these two degrees of freedom are necessary for capturing the characteristic features of the dynamics, and for revealing the physical origin of lattice response during potential energy sputtering processes. To date, there is little understanding about the relationship between physical mechanisms and dynamical consequences due the complex nature of the problems. At the current stage, simplified models, though seemingly crude, are necessary to study the explosion processes at the atomic level.

One of the key issues in modeling such a complex event is to treat the different time scales properly. First is the time for the surface to emit a large number of electrons. If this time interval is short enough compared to surface lattice motion, one can safely omit the electronic degrees of freedom of the projectile ion or treat it empirically. Previous theory suggests that a fast Coster−Kronig transition is the likely mechanism in ion−Si surface interactions.[35] In this model, the Si surfaces release electrons very quickly. Within 10 fs a substantial number of surface atoms can be ionized. The second time scale is that required for the rearrangement of the atoms and ions. The third time scale is for electrons in the substrate to hop from neutral regions to charged sites. It has been postulated[36−38] that the lifetime of multiple excitations in a semiconductor (or insulator) is longer than the lifetime of single excitation. This difference leads to a long neutralization time of the locally charged region on the surface. For example, the estimated neutralization time from experimental data is 0.87 ps for GaAs.[27,28] If this time is short, such as for a metal surface, the Coulomb explosion should be quenched. For an insulator such as SiO_2, the third time scale is long enough to be completely separated from the first two. For ionic and some covalent materials, the localized valence excitations provide the driving mechanism for nanoscale explosion on semiconductor surfaces. The relatively long lifetime of electron excitation is also closely related to a well-studied subject of surface desorption.[39,40]

In earlier simulations, based on the ICFS model,[33,34] 100−365 Si ions were generated at the Si(111) surfaces instantly, and the charge states were not allowed to change. This model provides meaningful results under two physical conditions: slow velocity of the incident ion and finite lifetime of the localized charge states in covalent materials.[36−38] The first condition allows surface ionization processes to occur approximately adiabatically; i.e., the ionization probability of a surface atom depends only on the distance between projectile ion and the surface. It also minimizes the influence of the kinetic energy of the incident ion (a Xe with $v = 10^3$ m/s has kinetic energy <1 eV). The second condition is necessary for observing Coulomb explosion in the ion−surface process. This condition could be satisfied in HCI−surface interactions in which electrons are ejected from both valence level and core level. Our previous simulations showed that for silicon systems, the violent stage of explosion lasts on the order of 100 fs.[33,34] If the number of positive ions is not greatly reduced in the ionized region during the first 100 fs (for Si), the ICFS model would be a reasonable first-order approximation to describe of the explosion process and subsequent dynamics. We have shown that even with the ICFS model, the sputtering outcome, as well as the dynamical behavior of the systems are very complex. Predictions of the time scale for shock wave formation and propagation and of sputtering yields, have provided valuable information and physical insights to the problems pertaining to HCI−surface interactions.

In this paper, we extend the ICFS model to include finite time charge buildup and charge relaxation. We describe the simulation results based on the new simultaneous ionization and charge migration (SICM) model that allows finite time surface ionization and surface ion migration simultaneously. Again, this modified model requires slow velocity of the projectile ion and finite lifetime (>10 fs) of localized charge states based on the multihole excitations among valence electrons.[36−38] The repulsive interactions among surface ions remain Coulombic as before. However, the time for ionizing the surface is allowed to be finite and the ions and atoms are allowed to change their charge states in a statistical manner. Effects due to such charge relaxation[20,27,28] can be included to a certain extent. The switching of charge states of the particles introduces effectively different mechanisms equivalent to defect migration in addition to pure Coulomb explosion. We report detailed results from MD simulations based on this modified model. Physical properties and dynamics consequences of the systems are studied by detailed analyses of phase-space trajectories. In particular, the time evolution of energy distribution, shock wave propagation, secondary ions emission, and amorphous formation are described quantitatively.

The current model and simulations therefore serve dual purposes: first, to investigate the processes in which surface

ionization could be the predominant mechanisms for potential energy sputtering which represents a variety of experimental results;[2,4−6,15,23,25,27,28,30−32] and second, to bridge the gap between the pure Coulomb explosion model and other bond-breaking models that are proposed for various systems. Thus, the electronic excitation, ionization, and the consequent dynamics of atoms can be treated within a unified theoretical framework. Furthermore, since the Coulomb repulsion is the fundamental interaction that underlies bond-breaking, the investigations in this study provide a zeroth-order approximation to various types of surface explosions caused by electronic excitations.

II. Modeling and Simulations

a. **Potential Energy Functions**. Choosing proper potential energy functions for each type of interatomic interaction is a crucial step in the MD simulations. In our studies, the Tersoff potential,[41] which provides relative reasonable description for both crystalline and amorphous semiconductor materials,[41] is employed to describe the Si−Si interaction. Because the energy scale involved in the simulation is substantially higher than thermal energy, the Tersoff potential thus serve the purpose to describe the formation of nanosize amorphous region in a Si surface. In order to describe the interactions between Si and Si^+ atoms, we combine information from experimental measurements and first-principles calculations[33,42,43] on Si−Si and Si−Si^+ dimers. These data are then fitted by a function of the form

$$V(r_{ij}) = \epsilon\left[\left(\frac{\sigma}{r_{ij}}\right)^{12} - \left(\frac{\sigma}{r_{ij}}\right)^{4}\right] \tag{1}$$

The function $1/r^4$ term is the proper asymptotic form for the interaction of the charge (on Si^+) and the induced dipole (on Si). The parameters σ and ϵ are 3.69 a_0 and 9.17 eV, respectively. The interaction between two Si^+ ions is taken simply as $1/r$ which is a crude approximation for the positively charged region. Note that this model potential does not distinguish valence electrons from core electrons. However, the physical mechanism is from the localized multihole multihole valence excitations.

b. **Changing Electronic States**. The model which we developed differs from conventional MD methods: Through the course of simulation, the electronic state of an atom or an ion is allowed to change from one to another, thus changing the interatomic potentials. In this study, two channels exist for a particle to change its state: first through direct ionization, and second through charge switching between Si and Si^+ atoms. Regarding the first channel, the ionization probability is taken to be proportional to

$$\Lambda_1 = \gamma e^{-(r_{ic}^2/r_\sigma^2)} \tag{2}$$

where r_{ic} is the distance of ith atom on the surface and the center of the projectile ion that is moving down toward the surface, γ and r_σ are constants. The ionization rate is now an adjustable function, and the probability of ionizing an surface atom depends on its location. This ionization function generates, over a finite period of time, an initial ionic region (positively charged) closer to the experimental situation than the model previously used for generation of such region,[33,34] in which the ions were instantaneously created in a well-defined hemisphere. Note that the charging probability is not a function of the velocity of the projectile ion. This approximation is justified for slow ion−surface collisions in which the charge transfer process could be represented by an adiabatic picture according to Landau and Zener.[44] In slow HCI−surface collisions, the velocity of the HCI could be as low as $<10^4$ m/s. At this velocity, an ion moves 1 Å in 10 fs which is the time scale for neutralization of the incident ion. The survival probability of the ion decays exponentially as the velocity decreases.

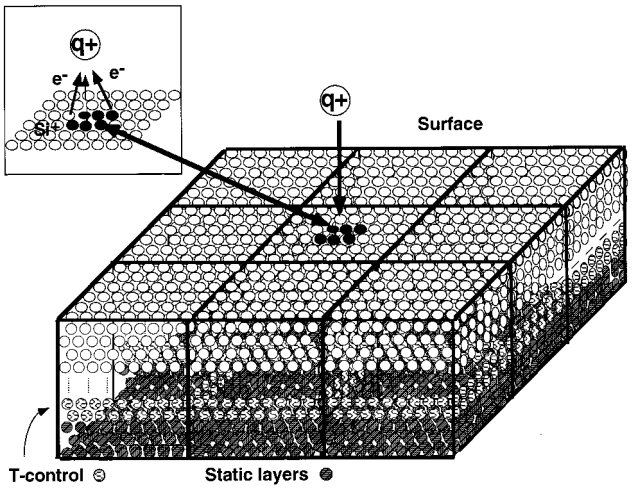

Figure 1. Schematic of simulation: the unit cell is repeated in the *x*- and *y*-direction. Note that the cells are not drawn in the exact proportion used in the simulations. Four types of particles are represented: dynamic Si atoms (open circles), thermal atoms (lightly shaded circles), static atoms, (heavily shaded circles), and Si^+ ions (filled circles), respectively. The projectile is a highly charged ion of charge state q^+.

The second charge transfer process which we include in our simulation is the charge exchange between Si and Si^+ atoms. In order to describe this process, we use the distribution function

$$\Lambda_2 = \frac{0.5 + \beta E_{ij}}{1 + e^{\alpha(r_{ij}-r_0)}} \tag{3}$$

where E_{ij} is the projection of the electric field at the ith ion due to all other ions in the direction of $\mathbf{r}_{ij}$, and α, β, and r_0 are constants. The physical picture of this probability distribution is the following: when a Si^+ ion approaches a Si atom *slowly*, the probability of charge transfer is 0.5 from symmetry consideration. In the presence of an electric field, the probability increases linearly as the electric field increases in the linear response limit. Thus, the factor βE_{ij} in eq 3 modulates the probability for charge transfer in the direction of $\mathbf{r}_{ij}$. We calculate the electric field at the ith ion and determine the probability as well as the direction for this positive ion to migrate. Migration of a positive charge is equivalent to transferring an electron in the opposite direction. The probability of charge transfer is modulated by a function of distance. By varying the parameters in the exponential function, a wide range of charge hopping, from nearest-neighbor hopping to nonlocal charge transfer, could be simulated. Equation 3 therefore allows neutralization of the positively charged region at a certain rate. The inclusion of this charge exchange is an improvement over the frozen charge approximation as used in our previously studies.[33,34] In this work, various rates will be investigated to study the relevance of charge transfer to HCI−surface processes.

c. **Simulation Details**. The simulations are performed on a Si(111) surface unit box containing 45 360 particles that are divided into four different regions: dynamical layers, static layers, temperature control layers, and a cluster with m ($m \leq 100$) ions. As shown in Figure 1, dynamical Si atoms are

represented by open circles, static atoms are in heavy shadow and remain at the bottom layer of the system, a few layers of atoms (lightly shade) between the dynamical particles and static particles are kept in thermal equilibrium with an external heat bath, and finally Si^+ ions are represented as the filled circles.

Before interacting with a HCI, the silicon sample is prepared at the desired temperature using thermalization techniques that mimic heat exchange between the system and an external heat bath, Once equilibrium is reached, heat exchange is limited to 1−2 layers just above the static layer, i.e., in the temperature control region. The temperature in all of the simulations here is held at 30−60 K, a very low temperature to ensure low carrier concentration and thus keeping the silicon substrate from conducting. Note that in our model, periodic boundary conditions (PBC) are applied only to neutral Si in the x and y directions. PBC are applied neither in the z direction nor to the ionic cluster which allows us to avoid the long-range interactions between ions in the neighboring unit cells, for systems with net charges.

The substrate is 106 a_0 thick and 261 $a_0 \times 226$ a_0 in the $x-y$ plane. With this size, a shock wave generated by 100 surface ions can travel 600−800 fs before it reaches the boundary or the static region in the z-direction. Tests show that the strength of the shock wave decays substantially after the first 100 fs and continues to decay at later times. Simulation after 1 ps is not affected significantly by the finite size of the system.

Each dynamic particle in the system follows Newton's equation of motion

$$m_i \frac{d^2\mathbf{R}_i}{dt^2} = -\nabla U(\mathbf{R}_1,\mathbf{R}_2,...\mathbf{R}_n) \tag{4}$$

where i, m, and $\mathbf{R}$ are the index, mass, and coordinates of the particle, respectively. U is the potential energy of the system that is determined by the nature of the interactions among the atoms. Note that in conventional MD simulations, U is not a explicit function of time t, as in eq 4. When ionization occurs, or when charge transfer occurs between a $Si-Si^+$ pair, the system moves from one potential energy surface to another and the coupling of these surfaces is treated statistically in the simulation.

An important quantity in particle−surface dynamical studies is the local temperature. Since the systems are far from the thermal equilibrium state during the collision process, the local temperature at time t is defined as the kinetic temperature that measures kinetic energy distribution of the particles. This time-dependent quantity is calculated by

$$\frac{3n-3}{2}k_b T = \sum_i^n \frac{1}{2} m_i v_i^2 \tag{5}$$

where k_b is the Boltzmann constant, m_i is the mass of the ith atom, and n is the number of atoms in the local region. Note that this temperature is completely different from the one used for temperature control. The atoms in the dynamic layers that are close to the collision center are not in thermal equilibrium with the rest of the system. In simulations of ion−surface processes, it is critical to introduce the concept of local temperature from the bulk temperature. The disturbance in the substrate could propagate into deeper layers of the surface via interatomic interactions. Energy dissipation to the external heat bath is achieved using temperature control in a region away from the violent explosion.

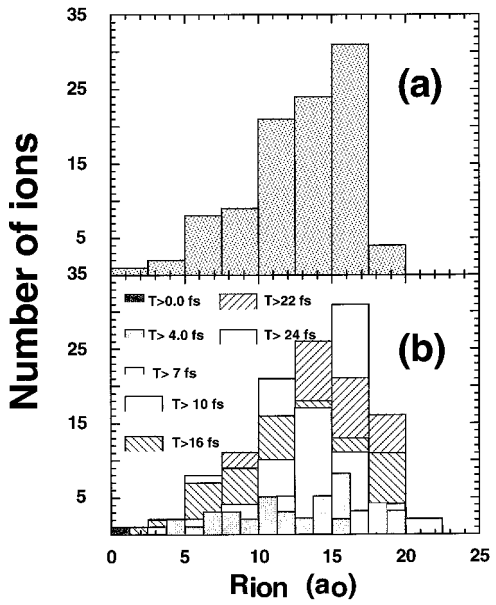

Figure 2. Initial ionization process: panel a represents the radial distribution of 100 ions that are generated instantly at $t = 0$; panel b depicts the development of the charged region at $t = 0$ (filled box), $t = 4.0$ fs (heavily shaded box), 7.0 fs (moderately shaded box), 10 fs (lightly shaded box), 16 fs (box with back slash), 22 fs (box with slash), and 24 fs (unfilled box). The histograms at earlier time are superposed on top of the ones at later time. The overall profile is the radial distribution of ions at $t = 24$ fs.

The total simulation time for most runs is approximately 1 ps (up to 5 ps for some systems). During this time, most of the important topological features of the craters are developed according to our previous experiences. The time interval Δt is 0.4 fs, but when Si or Si^+ change their charge states, we reduce Δt to one-eighth of its value for eight time steps to rebuild the predictor−corrector expansions.[45] We find that this procedure is very important for propagating the equations of motion correctly.

As a HCI approaches the surface, the number of surface ions gradually increases from 1 to m and the switch is turned off to prevent further ionization. The positive charges are moving away from each other via charge flow (eq 3) as well as via Coulomb repulsion. In the next section, we will discuss the implication of charge flow and its dynamical consequences.

III. Results

Four simulation runs, I−IV, were carried out in order to study the sputtering dynamics and thermal dynamics of the system. Each one reflects certain aspect of the underlying theoretical assumptions and predicts the outcome under given physical conditions. In simulation I, 100 surface ions are generated within 24 fs and $\beta = 0.2$ in eq 3. Simulation II uses same value of β, but the time for surface ionization is reduced to zero. Simulation III differs from II by using $\beta = 0.4$. Finally, in simulation IV the same parameters are used as in II at the beginning. However, β is set to zero after 100 fs.

a. Charge, Local Properties, and Shock Wave. In simulation I, the surface is charged up to 100 ions within the first 24 fs. The initial ionization profile is depicted in Figure 2. Panel a shows the charge distribution of 100 ions in a hemisphere of $R = 20$ a_0 at $t = 0$, a situation corresponding to the ICFC model used previously,[33,34] where the whole ionized region is created at once. Panel b shows the ionization over the first 24 fs using

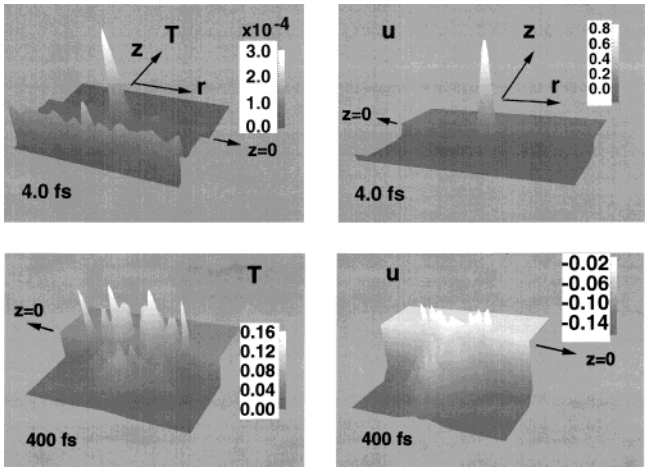

Figure 3. Snapshots of temperature (left two panels) and potential energy (right two panels) distributions at $t = 4.0$ fs (upper two panels) and $t = 400$ fs (bottom two panels). The local properties are averaged in the $x-y$ plane. The top surface layer is located at $z = 0$ as marked in one of the diagrams (upper left).

the present model where charging of the surface occurs gradually as the HCI approaches the surface (eq 2). The charged region develops from one ion at $t = 0$ that is represented by the black block to 100 ions at $t = 24$ fs that are represented by white blocks. The distributions corresponding to intermediate states are shown in blocks of different shades, where the dark to light shading represents the increase of the number of charged particles. The earlier distributions are superposed on latter ones for a better view of the temporal development. As seen in the figure, the profile of panel b is somewhat different than that of panel a.

Figure 3 displays snapshots of distributions of the temperature, T, and the local potential energy, u (energy per unit volume), of the system at different times. These quantities are averaged over the azimuthal angle φ in the $x-y$ plane and are plotted as a function of z and r ($r = \sqrt{x^2+y^2}$). The upper two panels are snapshots taken at 4.0 fs when 22 ions are generated, and the two bottom panels are at 400 fs. As seen in the figure, the peak value of temperature at 4.0 fs is within thermal energy, approximately 900 K. The peak value of the potential energy at that time is roughly positive 20 eV and is mainly due to the Coulomb energy. Both the temperature distribution T and the potential energy density distribution u indicate a very localized and smooth peak centered at the charged region. The major part of the system remains cold and undisturbed. At 400 fs, we observed the severe influence of the HCI−surface interactions. The peak value of T is now 48 000 K (300 $K = 9.55 \times 10^{-4}$ au) which comes from the high kinetic energy of the ions above the surface. (At $t = 400$ fs, many ions are repelled from the surface. Ions that are further than 10 a_0 above the surface are not included in Figure 3.) The temperature peaks in the substrate are approximately $^1/_3$ to $^1/_2$ of 48 000 K, which means quite high values as well. The potential energy, u, at 400 fs, is basically below zero, indicating substantial decay of Coulomb repulsion as distance between surface ions increases. Still, the substrate has a visible increase of potential energy.

Figure 4 depicts the temperature rise in a series of concentric hemispherical shell in the substrate. The radii of these hemispheres are 10, 15, 20, 25, 30, 35, 40, and 45 a_0. From the figure, we observe that the time interval for the temperature increase in each of the shells is very short. The average speed of the temperature propagation is estimated to be over 22 km/s

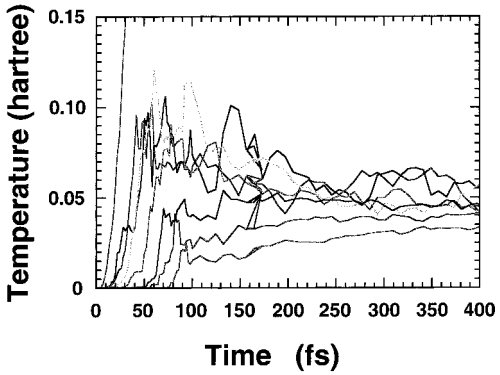

Figure 4. Temperature as functions of time in a set of concentric hemispheric shells that are centered at (0,0,0). Note that 9.55×10^{-4} hartree = 300 K so 0.1 hartree corresponds to more than 3×10^4 K. The distance between the center of the hemispheres and the outmost shell is 45 a_0. The speed of shock wave propagation is measured from the diagram to be ~22 km/s.

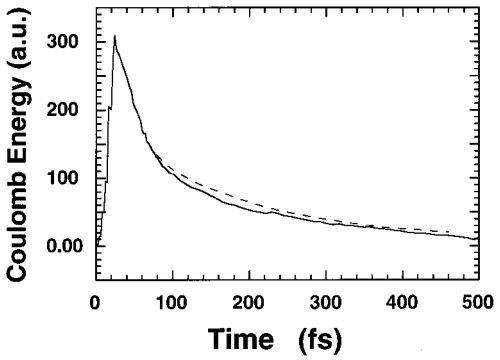

Figure 5. Coulomb energy as a function of time in the system with 100 ions. The solid curve is results from the first simulation and dashed curve is from the simulation, in which the charge flow is turned off at $t = 80$ fs.

(3−4 times of the speed of sound in solid silicon, which is ~5−6 km/s), which indicates shock wave propagation. Similar phenomena have been observed in previous HCI−Si (111) model studies[33,34] as well as during cluster−Si(111) surface collisions at high initial velocities ($v > 5$ km/s) and other cluster−surface collision processes.[46] Compared to the ICFS model,[33,34] the peak values of the temperature are slightly lower in the current study, but the strength of the shock wave decays slightly slower over a similar distance from the center than in the case of a pure Coulomb explosion. The more uniformly spatial distribution of energy is due to the charge propagation that releases part of the stress from inner shells to outer shells. At later times, all temperatures converge to the same value, as expected.

b. Energetics and Crater. The Coulomb energy is shown in Figure 5, in which the solid line depicts the rise and fall of the repulsive potential among all the ions. We will explain the dashed line later. The peak value is approximately 310 hartree (~8.7 keV), which is 40 hartrees lower than in the simulations using 100 ions in a hemisphere created all at once. The time for the energy to decay to e^{-1} of its peak value is approximately 65 fs, 30 fs shorter compared to the ICSF model.

At 800 fs (not shown in Figure 5), the total number of Si particles that have left their original locations in the substrate is measured to be 318 (including 25 ions). The criterion for secondary particle emission used here is that these particles are at least 10 a_0 above the top layer of the surface. Using the same

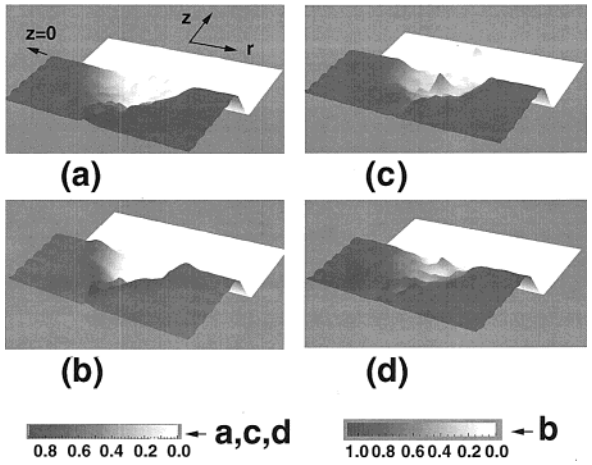

Figure 6. Snapshot of craters at $t = 800$ fs. The density distributions of the systems are displayed in the same way as in Figure 3. Craters created from simulation 1, ICSF model simulation; simulations 3 and 4 are shown in panels a−d, respectively.

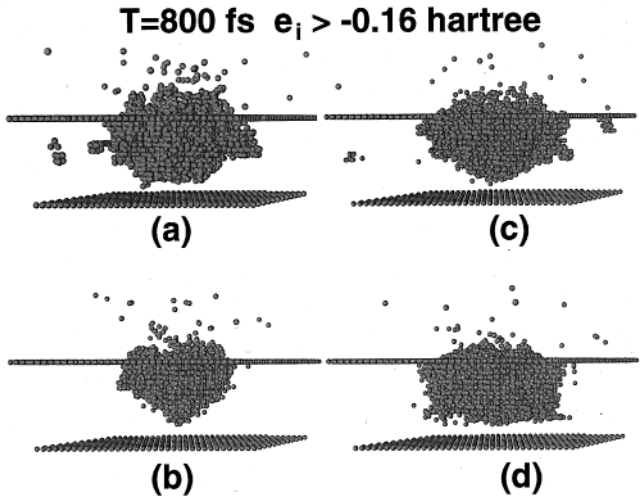

Figure 7. Snapshots of the amorphous pockets at $t = 800$ fs. Particles shown in the diagrams have energy value > -0.16 hartree which is ~0.3 eV higher than the value of an atom in the undisturbed Si substrate. Panels a−d display the shape and size of these pockets generated in simulation 1, simulation based on the ICSF model, simulation 3, and 4, respectively.

criterion, in the ICFS model, 201 particles (including 33 Si^+ ions) at 800 fs are ejected. Note that the ratio of ion to neutral decreases from 0.20 (the ICSF model) to 0.09 (current model). The shape of the crater can be seen in the upper left panel of Figure 6 (where the particle density is averaged over $x-y$ plane), which is similar to the one generated by the ICSF model (bottom left panel). The difference between the two craters is the residue and the roughness in the center of the crater in the current model.

We further analyze the surface damage by displaying all the particles whose energy (kinetic+potential) is higher than −0.16 au (or −4.35 eV), i.e., approximately 0.3 eV above the energy of an undisturbed atom in the substrate. Figure 7 depicts the particles that surround the crater at 800 fs. Panels a and b are snapshots for the current model and the ICFS model, respectively. Besides the atoms in the top layer (which have always higher energy than the bulk atoms) and the atoms in the static layer (at the bottom), other particles form amorphous pockets that have similar shapes in the two cases. However, it can easily be seen that the size of the pocket in panel a is bigger than the one in panel b, indicating more severe surface damage.

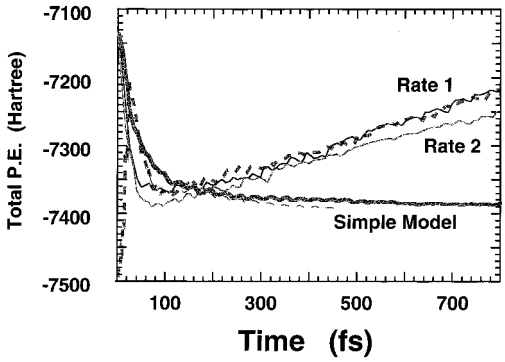

Figure 8. Total potential energy in a unit cell of the substrate as functions of time. Results from simulations 1−4 and the ICSF model are depicted in thick dashed line, thin dashed line, thin solid line (rate 1), thin solid line (rate 2), and thick solid line, respectively.

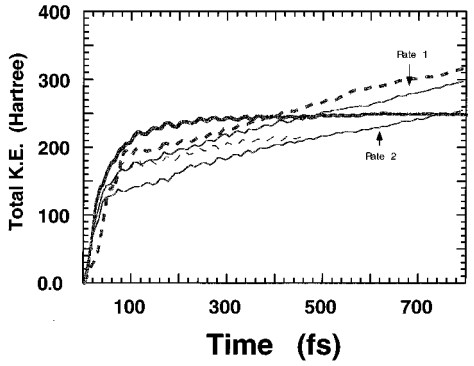

Figure 9. Total kinetic energy in a unit cell of the substrate as functions of time. Results from simulations 1−4 and the ICSF model are depicted in thick dashed line, thin dashed line, thin solid line (rate 1), thin solid line (rate 2), and thick solid line, respectively.

In order to understand these outcomes, we calculated the total mechanical energies, potential energy (Figure 8) and total kinetic energy (Figure 9), of the systems as functions of time. The thick dashed line and thick solid line represent the current model and the ICFS model, respectively. The significantly different behaviors obtained by the two model are clearly observed. In Figure 8, the total potential energy from the ICFS model decreases monotonically as a function of time. After the first 100 fs, the curve becomes flat, which indicates that at that time the Coulomb repulsion is substantially weakened. The current model, on the other hand, corresponds to a situation in which the potential energy rises to a maximum value when the surface is ionized, then falls to a minimum (at ~80 fs) as a result of the combined effects of Coulomb repulsion and charge flow, and later increases again due to charge flow. This pattern indicates that beyond 80 fs, the dominant effect is not caused by the Coulomb repulsion, but rather originates from the charge migration. The energy to drive the ions into the system comes from the continuous HCI−surface interaction which is not included in eq 4. The kinetic energies in Figure 9 indicate that the current model results in a continuously increasing temperature although the initial raise of temperature from the current model (thick dashed line) is lower than that from the ICSF model (thick solid line). The difference is that the thick solid line saturates and the others do not.

At 800 fs, approximately 12 keV energy is deposited to the surface based on the current model. Note that the maximum Coulomb energy is 8.7 keV. This information will be further analyzed in the next section.

c. A Lower Bound for Sputtering Outcome. The precise time for the electronic deexcitation in the center of bombardment is unknown at this point. However, Auger cascades can last a few hundred femtoseconds. Since deexcitation is the source for gaining more energy of nuclear motion in Figures 8 and 9, the final sputtering yields as well as the size of the crater will depend on the time at which the charge hopping is turned off. In order to provide an estimation of the lower bound of the sputtering outcome, simulation II is performed. In this simulation the charge flow is turned off just at the minimum of the thick dashed curve in Figure 8. The sputtering yields at 800 fs are then reduced to 109 including 25 ions. The ratio of ion to neutral is 0.23.

The Coulomb energy among the ions during the bombardment is shown in Figure 5 (dashed line) as compared to that in the first simulation (solid line). The difference is small, again suggesting that the defect migration can cause severe surface damage. Further analysis of the energy distribution shows that more than 50% of the total Coulomb energy (8.7 keV) converts to shock wave propagation and amorphous pocket formation.

d. Effects of Initial Ionization and Transfer Rate. Simulations III and IV are performed to investigate the effects of finite time of initial ionization, and different charge hopping rates.

The first observation is that the finite time ionization does not suppress the sputtering. When the same charge flow rate is applied, the sputtering yields at 800 fs, coming from the instant initial ionization, are found to be 267 including 21 ions, somewhat smaller than that in the first simulation, but larger compared to the ICSF model. The ion-to-neutral ratio is again 0.09. The crater at 800 fs is shown in panel c of Figure 6 and the amorphous pocket in panel c of Figure 7. Both the crater and the pocket are similar to the ones in the first simulation. However, there are subtle differences between the results form the two models, such as more residue atoms are generated in the center of the crater (Figure 6, panel c), in the third simulation, and (of less significance) differences in the detailed shape of the amorphous pockets (Figure 7, panel c).

The difference in the sputtering yields can again be interpreted in terms of energy. The thin solid line in Figure 9 marked by rate 1 depicts the kinetic energy of the system. The difference between the first simulation and the third results in different sputtering yields, while the potential energy curves almost coincide with each other (see Figure 8).

In the fourth run, we keep the same initial conditions as in the third run but increase the rate for charge flow. The sputtering yield is reduced to 160 including 16 ions, significantly smaller than the yields from simulations 1, 3, and the ICSF model, but higher than case 2. More residue atoms in the crater are observed (Figure 6, panel c). The ion-to-neutral ratio is 0.11, close to the other cases, in which charge hopping is allowed. The potential and kinetic energies of the system are given by the thin solid line marked rate 2 in Figures 8 and 9. As can been seen, both curves are significantly below cases 1 and 3. The kinetic energy is also below the ICSF model (Figure 9) for most of the time but catches on later while potential energy is above the ICSF model by a large amount. This portion of energy is not used to eject particles from the substrate; instead, it is responsible for the formation of a large amorphous pocket in the substrate (see Figure 7, panel d).

Figure 10 depicts the Coulomb energies for the ICSF model (the dot-dashed line), simulation 3 (dashed line), and 4 (the solid line). The biggest deviation of case 4 from the ICSF model is approximately 50−60 hartrees and occurs at times between 40 and 80 fs.

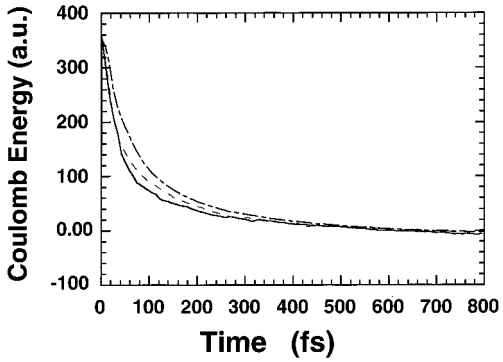

Figure 10. Coulomb energies of the systems as functions of time, from the ICSF model (dotted-dashed line), and simulations 3 (dashed line) and 4 (solid line). The significant deviations are observed in the early stage of explosion. At later times, all curves converge to zero.

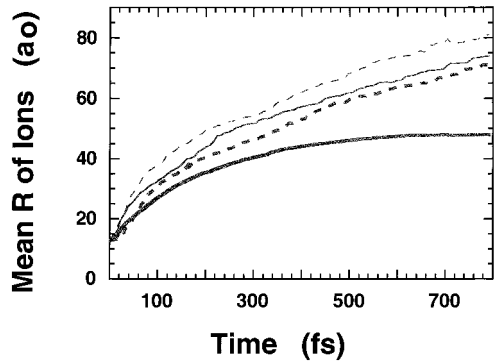

Figure 11. Mean radius of all ions as a function of time in simulations 1 (thick dashed line), 3 (thin solid line), 4 (thin dashed line), and the ICSF model (thick solid line). These curves provide the qualitative information on charge migration caused by Coulomb repulsion as well as by charge hopping.

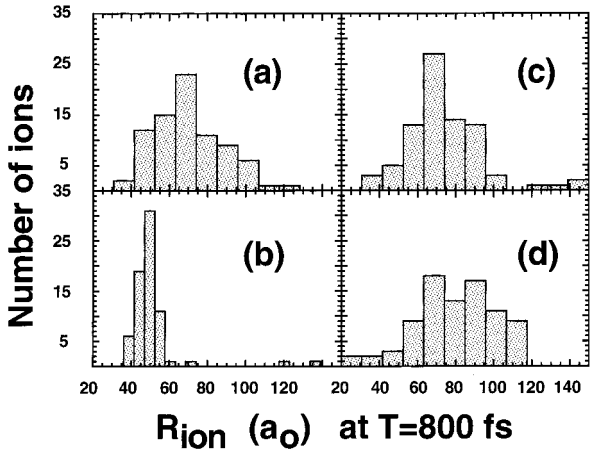

Figure 12. Radial distribution of ions at 800 fs. Panels a−d correspond to simulation 1, the ICSF model, simulations 3, and 4, respectively. A narrow distribution is observed in the ICSF model while simulation 4, which has the fastest charge flow, gives rise the most even distribution among all four cases.

Finally, we compare the charge distribution as a function of time. Figure 11 shows the time-dependent average radii of all the ions from the different simulations, the ICSF model (thick solid line), case 1 (thick dashed line), case 3 (thin solid line), and case 4 (thin dashed line). As expected, the ICSF model gives rise to a relatively slower charge migration. The extra speed is a result of charge hopping. Figure 12 displays the radial distribution at 800 fs. Panels a−d are case 1, the ICSF model, case 3, and 4, respectively.

IV. Conclusions

Several phenomena in surface nano-explosion upon HCI−surface interaction, some contradicting intuition, are observed in our model MD simulations that incorporate electronic degrees of freedom empirically and in a statistical manner. The finite time (on the order of tens of femtoseconds) during which the surface ions are generated does not suppress but enhances slightly the sputtering yield compared to the case in which ionization takes place instantaneously. The inclusion of charge flow can either increase the yields or reduce the yields, depending on the rate of the flow. The physical origin of the rate dependency is the competition between kinetic and potential energies. The process with higher increase of kinetic energy in the first 100 fs gives rise to higher yields. When the rate of charge flow reaches a critical value, the sputtering yields begin to decrease because the kinetic energy of the system is not high enough to eject more particles. Thus, results from our simulation model will also correspond to the experimental situation, in which Coulomb explosion is substantially quenched.

Charge hopping introduces a new mechanism that causes surface defects, in addition to pure Coulomb explosion. Compared to the pure Coulomb explosion process, the craters that are created via both mechanisms have similar features as generated from the ICSF model, but contain a small number of residue atoms. Shock wave propagation is also observed during the explosion processes based on the current model. Its strength is more evenly distributed spatially due to charge flow.

Over 50% of the initial Coulomb energy is deposited to the substrate. Part of the energy converts to the shock wave propagation, but the larger portion of energy is stored in the amorphous pocket that is developed around the crater, during the nano-explosion. When the rate of charge flow increases, more energy is converted to form the amorphous pocket, thus ejecting fewer atoms. The observation and analysis of the amorphous pockets explains partially the missing energy estimated by experimental measurements on electron emission, X-ray, ejected atom and ions, and current flow.[25]

The proposed model and the simulation results are availed when the localized excitations survive over a short time period on the order of 100 fs. Evidently, this is not the case corresponding to single ionization in which the charge can be completely delocalized. Earlier research does indicate that multiple holes can have longer lifetime in the covalent bond materials.[30−32,36−38] The evidence for localized two-hole valence electrons has been seen in the valence Auger spectra.[36] More recent research also indicated that electron−hole pairs in Si can have 100 fs lifetime when a large amount of them are all together. While the exact nature of electronic excitation in the semiconductor materials still remains unknown to a great extent, experimental evidence indicates that the surface atom/ion emission as well as surface modification does occur. Our goal is to provide the dynamical outcomes qualitatively based on a given model that describe a possible physical mechanism. Currently, we are performing new simulations to investigate processes in which other mechanisms such as bond breaking are more dominant than Coulomb repulsion. Our preliminary results on bond breaking already indicate that the surface explosion due to such mechanism is characteristically different. Detailed and systematic simulations are underway, and results have been reported recently.[47] (Coincidentally, similar simulation techniques have also been applied to study fast-ion (low charge)−matter interactions.[48]) A model containing both bond breaking and ionization is under development.

Finally, we should point out that important processes such as Auger cascades, resonant states, and neutralization of ions are not included explicitly in our model. In particular, the Auger core−valence−valence (CVV) line shapes had been used to probe the existence of the localized two-hole excitation.[49] The effects of some of these processes are partially included via finite charging process and the large number of surface ions. Given the situation in which dynamics of nuclei is yet to be understood even for a simple two-state (ground state and the charge state) model, inclusion of complicated electronic excitations could make problems intractable at this state of development. Construction of a comprehensive model that encompasses a rich array of physical mechanisms in the ion−surface interaction is our ultimate goal. This study and our current ongoing study of lattice dynamics caused by bond breaking are stepping stones for establishing such a sophisticated model for HCI−surface bombardment.

Acknowledgment. The authors gratefully acknowledge Dr. Gillaspy, Dr. Schenkel, Dr. Hamza, Dr. Schneider, and Dr. Landman for helpful discussions, the Department of Energy (under contract DE-FG02-97ER45660) for supporting this work, and The Wenner-Gren Foundations for partial support of a postdoctoral fellowship. The simulations were performed using computer facilities at the NIST Computing Center, and the graphics were produced in the QVS-Quantum Theory Project, University of Florida.

References and Notes

(1) Schenkel, T.; Barnes, A. V.; Hamaza, A. V.; Schneider, D. H. *Phys. Rev. Lett.* **1998**, *80*, 4325. Schenkel, T.; Briere, A. A.; Barnes, A. V.; Hamaza, A. V.; Bethge, K.; Schmidt-Böcking, H.; Schneider, D. H. *Phys. Rev. Lett.* **1996**, *78*, 2481.

(2) Schenkel, T.; Briere, M. A.; Hamaza, A.; Schach von Wittenau, A.; Schneider, D. H. *Nucl. Instrum. Methods. Phys. Res.* **1997**, *B125*, 153. Schenkel, T.; Barnes, A. V.; Hamaza, A. V.; Schneider, D. H. *Euro. Phys. J.* **1998**, *D1*, 297.

(3) Donets, E. D. *Rev. Sci. Instrum.* **1998**, *69*, 614.

(4) *Acta Phys. Hung., New Ser., Heavy Ion Phys.* **1996**, *3*, 229. Schneider, D. H. *Hyperf. Interact.* **1996**, *99*, 47.

(5) Park, D. C.; Bastasz, R. Schmieder, R. W.; Stöckli, M. *J. Vac. Sci. Technol.* **1995**, *B13*, 941.

(6) Gillaspy, J. D.; Agilitskiy, Y.; Bell, E. W.; Brown, C. M.; Chantler, C. T.; Daslettes, R. D.; Feldman, U.; Hudson, L. T.; Laming, J. M.; Meyer, E. S.; Morgan, C. A.; Pikin, A. L.; Roberts, J. R.; Ratliff, L. P.; Serpa, F. G.; Surga, J.; Takas, E. *Phys. Scr.* **1995**, *T59*, 392.

(7) Morgan, C. A.; Serpa, F. G.; Meyer, E. S.; Gillaspy, J. D.; Sugar, J. R.; Brown, C. M.; Feldman, U. *Phys. Rev. Lett.* **1995**, *74*, 1717.

(8) Schneider, D.; Church, D. A.; Weinberg, G.; Steiger, J.; Beck, B.; McDonald, J.; Magee, E.; Knapp, D. *Rev. Sci. Instum.* **1994**, *65*, 3472.

(9) Knapp, D. A.; Marrs, R. E.; Elloitt, S. R.; Magee, E. W.; Zasadzinski, R. *Nucl. Instrum. Methods* **1993**, *A334*, 305.

(10) Schneider, D. H.; Briere, M. A.; McDonald, J.; Biersack, J. *Radiat. Effect Defects Solids* **1993**, *127*, 113.

(11) Schneider, D.; Clark, M. W.; Penetrante, B. M.; McDonald, J.; Dewitt, D.; Bardsley, J. N. *Phys. Rev.* **1991**, *A44*, 3119.

(12) Bardsley, J. N.; Penetrante, B. M. *Comments At. Mol. Phys.* **1991**, *27*, 43.

(13) Schneider, D.; DeWitt, D.; Clark, M. W.; Schuch, R.; Cocke, C. L.; Schmieder, R.; Reed, K. J.; Chen, M. H.; Marrs, R. E.; Levine, M.; Fortner, R. *Phys. Rev.* **1990**, *A42*, 3889.

(14) Levin, M. A.; Marrs, R. E.; Henderson, J. R.; Knapp, D. A.; Schneider, M. B. *Phys. Scr.* **1988**, *T22*, 157.

(15) Sporn, M.; Libiseller, G.; Neidhart, T.; Schmid, M.; Aumayr, F.; Winter, H. P.; Varga, P. *Phys. Rev. Lett.* **1997**, *79*, 945.

(16) Eccles, A. J.; van den Berg, J. A.; Brown, A.; Vickerman, J. C. *Appl. Phys. Lett.* **1994**, *49*, 188.

(17) Neidhart, T.; Pichler, F.; Aumayr, F.; Winter, H. P.; Schmid, M.; Varga, P. *Phys. Rev. Lett.* **1995**, *74*, 5280.

(18) Aumayr, A.; Kurz, H.; Schneider, D.; Briere, M. A.; McDonald, J. W.; Cunningham, C. E.; Winter, H. P. *Phys. Rev. Lett.* **1993**, *71*, 1943.

(19) Aumayr, F.; Kurz, H.; Schneider, D.; Briere, M. A.; McDonald, J. W.; Cunningham, C. E.; Winter, H. P. *Phys. Rev. Lett.* **1993**, *71*, 1943. Hughes, G.; Burgdorfer, J.; Folkerts, L.; Havener, C. C.; Overbury, S. H.;

Robinson, M. T.; Zehner, D. M.; Zeijlman, P.A.; van Emmichoven, Meyer, F. W. *Phys. Rev. Lett.* **1993**, *71*, 291.

(20) Bitensky, I.; Parilis, E.; Della-Negra, S.; Beyec, Y. L. *Nucl. Instrum. Methods* **1992**, *B72*, 380 and references therein.

(21) Morgenstern, R.; Das, J.; *Europhys. News*,**1994**, *25*, 3; Schmieder R. W.; Bastasz, R. J. *Proc. VIth Int. Conf. Phys. Highly Charged Ions, AIP Conf. Proc.* **1992**, *274*, 675.

(22) Aumayr, F.; Burgdörfer, J.; Verga, P.; Winter, H. P. Preprint.

(23) Schenkel, T.; Hamaza, A. V.; Barnes, A. V.; Schneider, D. H.; Banks, J. C.; Doyle, B. L. Preprint.

(24) Schenkel, T.; Schneider, M.; Hattass, M.; Newman, M. W.; Barnes, A. V.; Hamaza, A. V.; Cicero, R. L.; Chidsey, C. E. D.; Schneider, D. H. Preprints.

(25) Schenkel, T.; Hamaza, A. V.; Schneider, D. H.; et al. Private communication.

(26) Gillaspy, J. D.; et al. Private communication.

(27) Itabashi, N.; Mochiji, K.; Shimizu, H.; Ohtani, S.;. Kato, Y.; Tanuma, H.; Kobayashi, N. *Jpn. J. Appl. Phys.* **1995**, *34*, 6861.

(28) Mochiji, K.; Itabashi, N.; Yamamoto, S.; Ochiai, I.; Okuno, K. *Jpn. J. Appl. Phys.* **1994**, *33*, 7108.

(29) DeZwart, S. T.; Fried, T.; Boerma, D. O.; Hoekstra, R.; Drentje, A. G.; Boers, A. L. *Surf. Sci.* **1986**, *177*, L939.

(30) Itoh, B. *Nucl. Instrum. Methods Phys. Res.* **1997**, *B122*, 405.

(31) Stampfli, P. *Nucl. Instrum. Methods Phys. Res.* **1996**, *B107*, 138.

(32) Stampfli, P.; Bennemann, K. H. *Phys. Rev.* **1994**, *B49*, 7299. Stampfli, P.; Bennemann, K. H. *Appl. Phys.* **1995**, *A60*, 191.

(33) Cheng, Hai-Ping; Gillaspy, J. D. *Phys. Rev.* **1997**, *B55*, 2628.

(34) Cheng, Hai-Ping; Gillaspy, J. D. *Comput. Mater. Sci.* **1998**, *9*, 285.

(35) Limburg, J.; Das, J.; Schippers, S.; Hoekstra, R.; Morgenstern, R. *Phys. Rev. Lett.* **1994**, *73*, 786.

(36) Knotek, M. L. *Phys. Today* **1994**, *9*, 24.

(37) Schauer S. N.; Williams, P. *Phys. Rev.* **1992**, *B46*, 15452. Jennison, D. R.; Kelber, J. A.; Rye, R. R. *Phys. Rev.* **1982**, *B25*, 1384.

(38) MaddenH. H.; Hennison, D. R.; Traum, M. M. *Phys. Rev.* **1982**, *B26*, 896.

(39) Akpati, H. C.; Nordlander, P.; Lou, L.; Avouris, Ph. *Surf. Sci.* **1997**, *372*, 9; Jennison, D. R.; Sullivan, J. P.; Schultz, P. A.; Sears, M. P.; Stechel, E. B. *Surf. Sci.* **1997**, *390*, 112.

(40) For review see: *Desorption Induced by Electronic Transition DIET I*; Tolk, N. H., Traum, M. M., Tully J. C., Madey, T. E., Eds.; Spring-Verlag: Berlin, 1983. *Desorption Induced by Electronic Transition DIET III;* Stulen, R. H., Knotek, M. L., Eds.; Springer-Verlag: Berlin, 1987.

(41) Tersoff, J. *Phys. Rev.* **1988**, *B39*, 5566.

(42) Baerend, E. J.; Ellis, D. E.; Ros, P. *Chem. Phys.* **1973**, *2*, 41. Delley, B.; Ellis, D. E.; Freeman, A. J.; Baerend, E. J.; Post, D. *Phys. Rev.* **1983**, *B27*, 2132.

(43) Cheng H. P.; Ellis, D. E. *Phys. Rev.* **1989**, *B39*, 12469.

(44) Levine R. D.; Berstein, R. B. *Molecuar Reaction Dynamics*; Oxford University Press: New York, 1974.

(45) Allen, M. P.; Tildesley, D. J. *Computer Simulations of Liquids*; Clarendon: Oxford, UK, 1987.

(46) Du, M.-H.; Cheng, H.-P. Submitted for publication. Cleveland, C. L.; Landman, U. *Science* **1992**, *257*, 355.

(47) Hedstrom, M.; Cheng, H.-P. *Phys. Rev. B*, in press.

(48) Bringa E. M.; Johnson, R. E.; Jakas, M. *Phys. Rev.* **1999**, *B60*, 15107. Bringa, E. M.; Johnson, R. E.; Dutkiewicz, L. *Nucl. Instrum. Methods Phys. Res.* **1999**, *B152*, 267.

(49) Jennison, D. R. *Phys. Rev.* **1978**, *B18*, 6865.